Synergistic use of satellite thermal detection and science: a decadal perspective using ASTER

MICHAEL S. RAMSEY

Department of Geology and Planetary Science, University of Pittsburgh, 4107 O'Hara Street, Pittsburgh, PA 15260, USA (e-mail: mramsey@pitt.edu)

Abstract: Many volcanoes around the world are poorly monitored and new eruptions increase the need for rapid ground-based monitoring, which is not always available in a timely manner. Initial observations therefore are commonly provided by orbital remote sensing instruments at different temporal, spatial and wavelength scales. Even at well-monitored volcanoes, satellite data still play an important role. The ASTER (Advanced Spaceborne Thermal Emission Radiometer) orbital sensor provides moderately high spatial resolution images in multiple wavelength regions; however, because ASTER is a scheduled instrument, the data are not acquired over specific targets every orbit. Therefore, in an attempt to improve the temporal frequency of ASTER specifically for volcano observations and to have the images integrate synergistically with high temporal resolution data, the Urgent Request Protocol (URP) system was developed in 2004. Now integrated with both the AVHRR (Advanced Very High Resolution Radiometer) and MODIS (Moderate Resolution Imaging Spectroradiometer) hotspot monitoring programmes, the URP acquires an average of 24 volcanic datasets every month and planned improvements will allow this number to increase in the future. New URP data are sent directly to investigators responding to the ongoing eruption, and the large archive is also being used for retrospective science and operational studies for future instruments. The URP Program has been very successful over the past decade and will continue until at least 2017 or as long as the ASTER sensor is operational. Several volcanic science examples are given here that highlight the various stages of the URP development. However, not all are strictly focused on effusive eruptions. Rather, these examples were chosen to demonstrate the wide range of applications, as well as the general usefulness of the higher resolution, multispectral data of ASTER.

Monitoring of effusive volcanic processes from orbit using thermal infrared (TIR) data has been ongoing from the earliest days of the satellite era (Gawarecki *et al.* 1965; Friedman & Williams 1970; Scorer 1986). Ramsey & Harris (2013) more recently summarized the history of satellite-based thermal infrared (TIR) research of active volcanoes into four chronological themes based on technology development: (1) hotspot detection; (2) analysis of subpixel components; (3) heat/mass flux studies; and (4) eruption chronologies. These themes follow a predicable pathway based on the available technology and computer processing capabilities at the time of each study. As satellite TIR sensors continue to improve in spatial, temporal and/or spectral resolution, so does the paradigm of spaceborne volcanology. The ability of scientists to extract new informational types from precursory activity through to detailed analysis of the erupted products continues to grow exponentially. The simple detection of a new 'thermal anomaly' at a quiescent volcano marking the start of new activity gave rise to detailed analysis of the temperature distribution below the pixel scale, which then allowed more accurate modelling of flux rates and chronological descriptions of each eruptive phase.

During the past 50 years of satellite TIR data, a fundamental technological divide has separated these studies: the use of high temporal–low spatial resolution v. low temporal–high spatial resolution data. The former typically falls under a class of sensors designed primarily for weather and atmospheric studies, and includes the Advanced Very High Resolution Radiometer (AVHRR), the Geostationary Operational Environmental Satellite (GOES), the Along Track Scanning Radiometer (ATSR) and the Moderate Resolution Imaging Spectroradiometer (MODIS) instruments. These sensors commonly are designed with wide swath widths, a limited number of spectral bands and spatial resolutions of 1.0 km/pixel or larger, which results in temporal frequencies of minutes to hours. Although this class of sensor has existed since the earliest days of orbital measurements, there were few studies of active volcanic processes using these data because of the poor spatial resolution, low signal to noise (SNR) and the large amount of thermal activity required for detection by these early sensors (Williams & Friedman 1970; Scorer 1985). However, improved analysis techniques that have been designed to extract information below the scale of a pixel have now made these datasets invaluable for both rapid detection of new activity and analysis of timescale-dependent eruptive processes (e.g. Harris *et al.* 1997*b*; Wright *et al.* 2002*a*; Hirn *et al.* 2008). The other class of sensors

From: Harris, A. J. L., De Groeve, T., Garel, F. & Carn, S. A. (eds) *Detecting, Modelling and Responding to Effusive Eruptions*. Geological Society, London, Special Publications, **426**, http://doi.org/10.1144/SP426.23

have high spatial and low temporal resolution data, and include the Landsat and Satellite Pour l'Observation de la Terre (SPOT) series of instruments, the Advanced Spaceborne Thermal Emission and Reflection Radiometer (ASTER) and the sensors on the Earth Observing-1 (EO-1) spacecraft, to name just a few. These sensors commonly have a larger number of spectral bands and spatial resolutions of 100 m/pixel or smaller, but a temporal frequency of the order of days to weeks. However, the improved spatial resolution does allow more detailed studies of smaller-scale processes and a much lower thermal detected threshold (Harris *et al.* 1999). For example, these sensors are excellent at detecting early precursory activity. Unfortunately, the data do not have the ability to document ongoing rapid changes during any given eruption because of relatively infrequent sampling (e.g. a 16 day nadir repeat cycle for a sun synchronous orbit).

In the past decade, a fifth broad theme has arisen that could be added to the list of Ramsey & Harris (2013): that of the combined used of both instrument technologies in a sensor-web approach in order to capture multiple scales of activity at an erupting volcano (Duda *et al.* 2009; Davies *et al.* 2015). In the most straightforward implementation of this approach, high temporal resolution sensors are used for detection of new activity, and subsequently trigger rapid scheduling and acquisition of higher spatial resolution data from other sensors. With such a system in place, specific volcanic activity can be monitored using the high spatial resolution data to image small-scale changes and to validate the continuous stream of low spatial resolution data.

One such system is the Urgent Request Protocol (URP) Program, which has been operating as part of the ASTER sensor's operational scheduling since 2004 (Duda *et al.* 2009). The URP has been responsible for over 2000 additional scenes of active volcanoes during that time, which is approximately one new scene every 2 days. This is a vast improvement from the sensor's original nominal volcano observation strategy of between 4 and 18 images per year (one image every 90 or 20 days, respectively) for each of the world's active and potentially active volcanoes (Pieri & Abrams 2004; Urai & Pieri 2011). Moreover, recent improvements in the URP system have expanded the monitored area to the entire globe from the original region centred in the northern Pacific (Ramsey *et al.* 2004). In operation since 2011, this expanded URP system has provided detailed TIR and visible/near infrared (VNIR) ASTER data of new effusive eruptions (e.g. Tolbachik, Russia), as well as ongoing activity (e.g. Etna, Italy; Kilauea, Hawaii) (Ganci *et al.* 2015; Patrick *et al.* 2015).

Background

The ASTER sensor

The ASTER instrument is one of five on the United States National Aeronautics and Space Administration (NASA) Terra satellite launched in December 1999. ASTER was developed and built in Japan under the Japanese Ministry of Economy, Trade and Industry (METI) and has a combined science team of Japanese and United States investigators (Kahle *et al.* 1991). In the 15 years of operation, the data have been used to improve the understanding of numerous local- to regional-scale processes, including volcanic activity (Pieri & Abrams 2004; Urai 2004; Carter & Ramsey 2010; Ramsey *et al.* 2012). The instrument was designed with three spectral channels in the VNIR region (0.52–0.86 μm), six in the shortwave infrared (SWIR) region (1.6–2.43 μm) and five in the TIR region (8.13–11.65 μm), with resolutions of 15, 30 and 90 m/pixel, respectively (Yamaguchi *et al.* 1998). Unfortunately, SWIR data have not been acquired since 2009 due to a failed detector cooling system. On average, 518 scenes per day are obtained and, as of December 2014, a total of approximately 2.7 million ASTER scenes have been acquired, with more than 250 000 of those focused on volcanoes and volcanic activity.

Pieri & Abrams (2004) and Ramsey & Flynn (2004) described in detail the particular instrument characteristics that make ASTER well suited for volcanic observations. These include, to name only a few: multispectral TIR data; routine TIR data at night; high spatial resolution; variable gain settings to limit data saturation; and the generation of along-track digital elevation models (DEMs). In particular, the multispectral TIR data at a relatively high spatial resolution allow a variety of surface materials to be distinguished, and a complete understanding of the thermal and compositional mixing within a given pixel or region of pixels to be achieved (Scheidt *et al.* 2011; Ramsey *et al.* 2012; Rose *et al.* 2014).

ASTER is designed as a pointable instrument (up to 24° off nadir for the VNIR and 8.55° for the TIR), and therefore requires a fundamentally new approach towards the scheduling and management of the data observations. This flexibility in pointing and gain settings, in conjunction with the limited daily 8% duty cycle of ASTER, impose a complex prioritization of targets and a substantial scheduling requirement every orbit/day. Larger goals, such as compiling a global map of the land surface, are integrated with emergency/high-priority requests and larger science team acquisition requests (STARs), such as monitoring the world's volcanoes, global land ice and urban environments.

Therefore, daily observational plans are first simulated using complex scheduling software and then created for later upload to the sensor. Although this approach requires human intervention at several stages, it results in an improved level of flexibility and temporal sampling frequency compared to comparable previous missions (Pieri & Abrams 2004).

In the early days of the mission, acquired data had a latency period from acquisition to download availability of up to 2 weeks. This was due to the requirement that all raw data (level 0) were processed to level 1A/level 1B (radiometrically and geometrically corrected) in Japan. Level 0 data had to be shipped from the United States to Japan on magnetic tape for this processing and then shipped back again for archiving. This delay clearly made it impossible to quickly analyse data of extreme events and natural disasters, which require a more timely response. In recent years, this latency period has improved to several days as a result of the direct transfer of digital data to/from Japan and the elimination of the tapes. However, this smaller lag coupled with the required time needed to schedule and observe an event such as an ongoing volcanic eruption still meant that ASTER data were not timely enough as a response tool.

The expedited data system

The ASTER expedited data system (EDS) is a scheduling and processing plan initially enacted prior to the launch of Terra and designed to reduce this large scheduling/data processing latency. It was conceived as a policy tool that would allow both science teams a limited number of emergency requests per month (30 each for the USA and Japan). These are given the highest priority ensuring that the data are acquired (especially if there was a scheduling conflict with another preplanned observation). The raw EDS data are processed to L1A/L1B in the United States (for US-initiated requests) and immediately staged for quick download. This reduces the latency from acquisition to availability to as short as 2 h, which vastly improves ASTER's relevance for post-disaster assessment. From 2000 to 2004, the ASTER EDS averaged approximately 20 observations per month for the US Science Team, with approximately 20% of those being volcano-related. Over the next decade, after implementation of the URP Program, the number of EDS observations increased to 34 per month, with over half being volcano-related.

The ASTER volcano observation strategy

The ASTER science team acquisition requests (STARs) are also part of the original routine data acquisition and monitoring goals of ASTER (Yamaguchi *et al.* 1998). These STARs are created for science goals that require a large amount of data acquired numerous times over a multi-year timeframe. The original ASTER volcano observation STAR was designed to make routine observations over the world's volcanoes available to volcanologists as quickly as possible (Urai *et al.* 1999; Urai & Pieri 2011). The plan for this STAR subdivided the approximately 1000 active/potentially active volcanoes globally into categories based on activity. Observing strategies for individual volcanoes varied according to the historical frequency of their eruptive activity. Three classes (A, B and C) were created, with class A volcanoes having had several recorded eruptions during prior decade, class B volcanoes having had several recorded eruptions during the prior century and class C volcanoes comprising the remainder. There are 102 volcanoes in class A, with each observed every 48 days in the daytime and every 32 days at night; class B targets ($n = 222$) are observed once every 3 months, day and night; and class C volcanoes ($n = 640$) are observed only once every 6 months (Urai *et al.* 1999). This plan does provide for all volcanic centres on Earth to be imaged on a regular basis (a total of 6287 observations per year), with an annual average frequency of 19 scenes for each of the most active volcanoes (class A). An analysis of the volcano STAR observation success rate several years into the mission showed that the targets in class A were only being imaged, on average, 85% of the planned number; whereas those in the other classes were being observed slightly more often than planned (M. Urai pers. comm.). These averages are not adequate to provide rapid response assessment and to discriminate short-timescale activity (especially if one considers that a percentage of these scenes will inevitably be cloudy). Therefore, the ASTER Urgent Request Protocol Program was proposed as a means to improve the number of observations at these most active volcanic centres around the world (Ramsey *et al.* 2004; Duda *et al.* 2009).

The URP Program

Soon after the launch of Terra, ASTER began acquiring images of active volcanic processes, such as the 2000 eruption of Bezymianny volcano in Kamchatka, Russia that produced a large pyroclastic-flow deposit. The first ASTER TIR data revealed small-scale details on the extent, composition and cooling history following the eruption, and spurred interest in using ASTER for expanded volcano science in the northern Pacific region (Ramsey & Dehn 2004).

The ASTER URP system was conceived soon after as a synergistic approach that would take

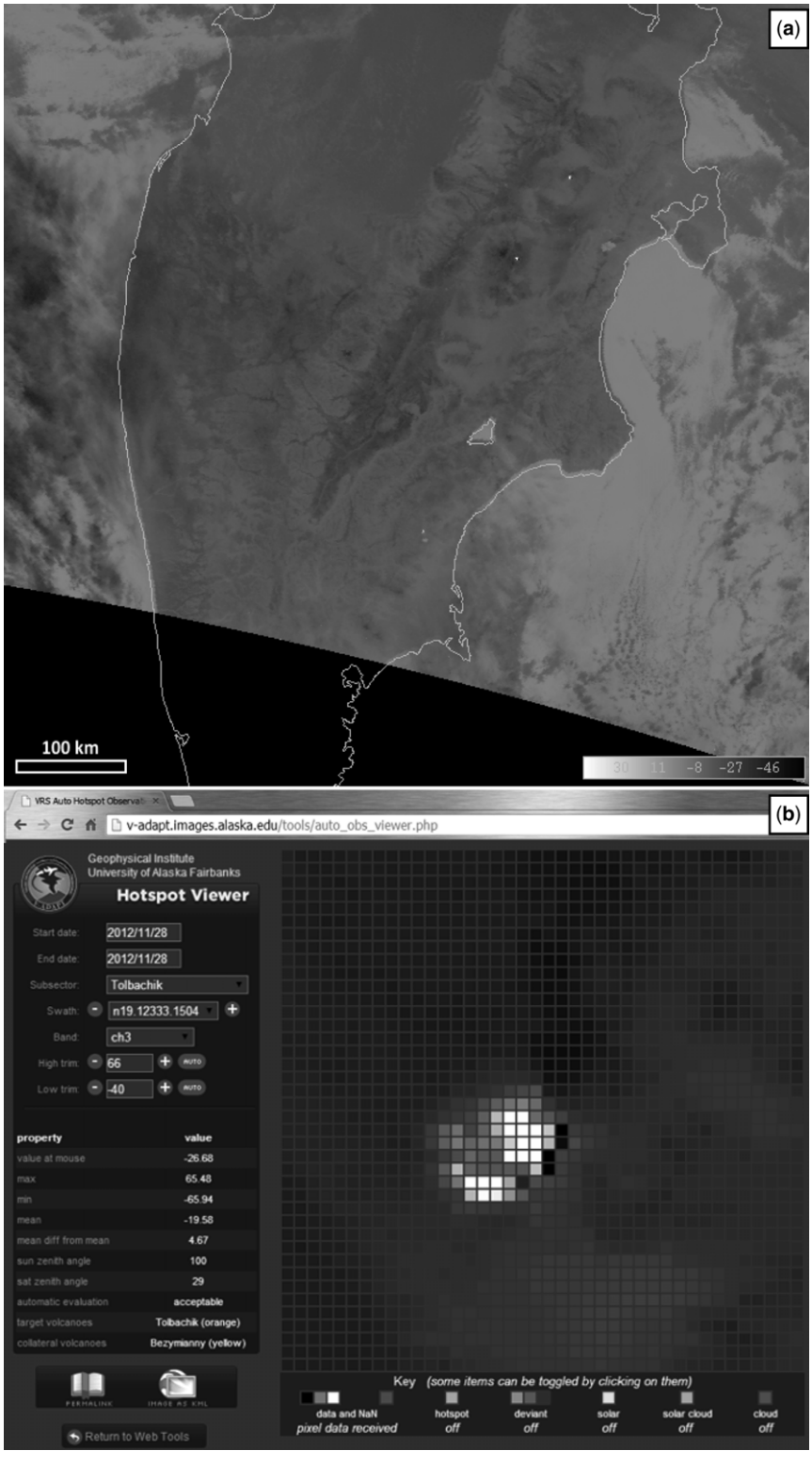

advantage of the best characteristics of both classes of satellite temporal resolution specifically for volcano monitoring and science. Initially tested as part of the integrated ASTER Science Team effort, the URP Program has now been supported by four competitive grant awards from NASA that started in 2004 and is currently funded until 2017. The initial design took advantage of an established satellite monitoring framework by the Alaska Volcano Observatory (AVO) and the University of Alaska Fairbanks (UAF) (Dean *et al.* 1998). That monitoring system was already well established, and had the software tools needed to rapidly scan AVHRR data from the Northern Kurile Islands, Kamchatka, the Aleutian Arc and south to the northern Cascades for thermally elevated pixels (Dehn *et al.* 2000). The first generation of the URP system relied on this infrastructure while developing new tools that would provide a rapid pathway for scheduling, collecting and processing ASTER data following a new detection in the AVHRR data. This programme developed a new complex interconnection between the University of Pittsburgh (UP), AVO, UAF, the NASA Land Processes Distributed Active Archive Center (LP DAAC) at the United States Geological Survey (USGS) Earth Resources Observation and Science (EROS) Center and the Jet Propulsion Laboratory (JPL), as well as the Earth Remote Sensing Data Analysis Centre (ERSDAC) in Japan. It also funded five field campaigns in Kamchatka for science and data calibration/validation, and in the process strengthened collaborations with the Russian Institute of Volcanology and Seismology (IVS) and the Kamchatka Volcanic Eruption Response Team (KVERT), supported four PhDs and three MS graduate degrees, and resulted in over 20 publications (e.g. Carter *et al.* 2007; Wilson *et al.* 2007; Rose & Ramsey 2009). The ongoing multi-agency arrangement, which is described in Duda *et al.* (2009) along with the details of the first several years of URP operation, has been highly successful.

Methods

The URP operational approach

Because of the typical data acquisition complexity of a scheduled instrument like ASTER, combined with the original constraints of the processing pathways and the limited expedited data volumes agreed to by the United States and Japan, the URP system is never able to be fully automated. Human intervention is still required to: (1) evaluate any initial false positive detections; (2) review the expedited request resulting from a valid detection; (3) approve it, contingent upon the upcoming acquisition schedule and the number of expedited scenes previously acquired that month; and, finally, (4) upload it into the upcoming ASTER schedule. Operationally, certain throttling constraints must also be placed on the URP system in order to eliminate compounding ASTER requests (i.e. new triggering requests arriving before the prior requested observation had been fulfilled) and ensure that the EDS limit of approximately 30 per month is not exceeded. One such constraint that arose was the implementation of a 10 day inhibit window at a particular volcano starting at the time of a new alert and continuing until the next URP request is triggered. With this in place, the temporal resolution of ASTER effectively only improved from 16 days (nominal) to 10 days (URP mode). However, every URP request is for a day–night pair and therefore two observations will occur separated by anywhere from 12 to 30 h. Furthermore, one must consider that without the URP system continually queuing up new requests every 10 days, the nominal operation schedule of ASTER virtually eliminates any possibility of one volcanic target being observed during every possible Terra overpass. That results in a frequency far worse than every 16 days, which occurs at many other (non-URP-monitored) volcanoes. Typically, several manual EDS observations are requested in these situations supplemented by the nominal ASTER volcano STAR and, therefore, several images are acquired every 4–6 months. Finally, at higher latitudes and during heightened urgency levels, this 10 day inhibit window reduces because of the overlapping orbit tracks of Terra, which can result in observational triplets (night–day–night) over a 48 h period, thus greatly improving the ability to resolve small-scale temporal changes (e.g. Rose & Ramsey 2009).

Once a volcano is identified as having an increased thermal output in the AVHRR data (see Dehn *et al.* 2000 for a complete description of the detection approach), an e-mail is sent to key URP participants with a link to the actual AVHRR image and a webpage that allows a cursory analysis to be performed (Fig. 1). This interaction typically takes 1–2 min at most and prevents false positives from being sent forward to the ASTER scheduling

Fig. 1. AVHRR data of Kamchatka, Russia shown with tools developed at the University of Alaska Fairbanks. **(a)** Subset of the band 3 (3.9 μm) AVHRR image acquired on 22 November 2009 at 20:02 UTC with hotspots denoted by the white arrows. **(b)** Hotspot Viewer web interface showing a 40 × 40 pixel area of a band 3 AVHRR image acquired on 28 November 2012 at 15:04 UTC and centred over Tolbachik volcano. The large multi-pixel anomaly was the result of the start of the new fissure eruption (see Fig. 8).

Table 1. *Monitored volcanoes in phase 3 of the ASTER URP project using MODVOLC as the URP triggering mechanism*

Volcano	Country	Volcano	Country
Ambrym	Vanuatu	Popocatepetl	Mexico
Cordon Caulle	Chile	Reventador	Ecuador
Erta Ale	Ethiopia	Ruiz	Columbia
Etna	Italy	Sakura Jima	Japan
Kilauea/Pu'u O'o	USA	Santa Maria	Guatemala
Nyamuragira	DR Congo	Semeru	Indonesia
Nyiragongo	DR Congo	Stromboli	Italy
Pacaya	Guatemala	Tungurahua	Ecuador
Paluweh	Indonesia	Yasur	Vanuatu

system. A confirmed thermal anomaly will then trigger an automated software system at the LP DAAC called the ASTER Emergency Scheduling Interface and Control System (AESICS), which was developed as part of the original URP Program. AESICS can also be tasked manually and has been used to plan the ASTER observations of many non-volcanic natural disasters over the years (e.g. Duda 2012; Duda & Abrams 2012). For URP requests, this part of the system pathway is fully automated and produces a completed scheduling request, which is automatically forwarded on to JPL for the final approval and official scheduling. The entire process from the initial trigger to awaiting final scheduling approval at JPL takes less than 5 min. However, the actual schedule planning and transmission to Japan can take from several hours up to 1 day depending on the timing of the incoming request and the availability of personnel to review it. ASTER is then tasked and the volcano is targeted at the next orbital overpass opportunity. Within 2–4 h of the data being acquired, all scientists involved are automatically notified and have immediate web-based access to the new scene. Any significant changes detected in the data are disseminated to the responsible monitoring agencies and the global community through e-mail and mailing lists. More detailed science analysis is then commonly performed over time and with the arrival of more datasets.

Expansion of the URP

In 2011, phase 3 of the URP system was undertaken, and this involved a considerable expansion in both the scope of coverage and the volume of data returned from ASTER. The URP implementation was integrated into the MODVOLC system, which monitors global MODIS data from the instruments on the Terra and Aqua satellites for changes in thermal output (Flynn *et al.* 2002; Wright *et al.* 2002*b*, 2004). The same basic approach used for the North Pacific monitoring was incorporated into the MODVOLC system with two significant changes. First, because the MODIS data are far less prone to noise compared to AVHRR and because the MODVOLC detection threshold is set fairly high, false positive detections are exceedingly rare (Steffke & Harris 2010). Therefore, manual screening of incoming alerts after a triggering detection is not required, thus making the process fully automated from the detection event through to the transmission to the LP DAAC and finally onwards to JPL. The second significant change is that the MODVOLC URP integration could not operate unconstrained globally owing to the large volume of data. Because the ASTER EDS was already nearing (or, at times, exceeding) the maximum number of scheduled scenes per month, a constraint was required on the number of MODIS monitored volcanoes. Ten volcanoes were initially chosen based on their prior high activity levels and as a test of the new MODIS/ASTER URP system. Once the number of new monthly URP requests from MODIS was determined, this list was allowed to expand to the current 18 volcanoes (Table 1). The limited number of MODIS-observed targets (in addition to the continued AVHRR URP monitoring in the entire North Pacific region) consistently produces expedited requests near or at the maximum monthly limit for ASTER (Table 2). However, there are several approaches being explored to refine and improve this constraint in order to either allow more targets to be added or allow the list to be continually modified so that new activity can be observed at volcanoes not currently on the list after no-longer-active volcanoes are removed.

Results

Data integration

The ASTER URP Program has been operational in some form since 2004, expanding from simple manual triggering of the expedited data system

Table 2. *Summary of ASTER volcano acquisition statistics over the past decade from the initial phase of the URP Program until present*

Year	URP phase	Days/volcano scene	Volcano scenes/ month	Volcano scenes/ month (%)
2004–05	1 (manual + URP)	5.5	5.5	21.6
2006–10	2 (AVHRR + URP)	2.3	13.1	40.0
2011–14	3 (MODIS + URP)	1.3	23.6	61.0

Each new phase is cumulative, meaning that by phase 3 all triggering mechanisms (manual, AVHRR and MODIS) are operating concurrently. In the current phase, the URP Program is now responsible for 61% of all the expedited scenes acquired by ASTER, resulting in a new volcano scene every 1.3 days on average.

(EDS) in the first year to routine near-automated global monitoring of the most active volcanoes by way of triggering from the AVHRR and MODIS sensors. The initial development of the URP is centred on a set of software and web-based tools at the LP DAAC, later called AESICS (Duda *et al.* 2009). AESICS allows a quick interface into the ASTER EDS and the ability to subsequently track those requests graphically using a Google Map interface (Fig. 2) and underlying statistical database. This system also allows testing to be performed in order to track the number of requests per month and how they are handled, as well as the success rate and the timing of both the request-to-scheduling and the scheduling-to-acquisition phases. Finally, AESICS serves as the core interface into which the future automated triggering requests from AVHRR and MODIS are inserted. This common request interface was developed, and is now used for all automated incoming requests from the AVHRR monitoring in the North Pacific and the global MODIS monitoring. It can also accept manual requests, as well as those from other orbital and/or ground-based triggering systems.

As a new triggering request is logged into the AESICS system, it is parsed, displayed on the map, and an official ASTER scheduling request is created and forwarded to the Jet Propulsion Laboratory. For any given 2 week period, the map interface shows new request targets in red, approved/scheduled requests in yellow and completed observations in green. Each of these is clickable in order to display more detailed information, including a link to the data record as well as the actual image, once acquired (Fig. 2a). The map interface can also be changed to display all URP targets acquired over certain time periods in order to track the overall success rate during that time (Fig. 2b, c).

Beginning in early 2004 at the start of the official funding for the URP project, AESICS was developed and used to ingest new targets manually based on known reports of active/ongoing eruptions. This phase of the programme centred almost entirely on the North Pacific region as the automated AVHRR triggering was also being developed at the University of Alaska. During the 2004–05 timeframe, the URP-based requests accounted for an average of 21.6% of the total expedited observations (Fig. 3). When the system was expanded (phase 2) to include both manual and AVHRR-based requests, URP-based observations of active volcanoes increased to 40.0%. Finally, in the current phase 3 with the MODVOLC triggering requests at 18 volcanoes globally (plus the AVHRR and manual requests), the system now produces 61.0% of all the expedited observations by ASTER (Table 2). This rate results in a new URP scene being acquired, on average, every 1.3 days or approximately 24 observations per month. The current system is, however, approaching the limit of monthly EDS scenes allowed using this rapid response approach, as well as the need to balance volcano observations with those of other emergency situations and natural disasters.

As the ASTER sensor approaches its fifteenth year in orbit, there is a growing desire to test new ideas, observation strategies and use the vast data archive to plan future mission concepts. One such observational change is to acquire a global TIR night-time map of the world's land surface and another is to further improve strategies for lowering the response time to natural disasters. It should be noted that all of these new data collection strategies are being attempted in an era of declining funding in both the United States and Japan, however. The URP Program has been renewed with funding until 2017 and a primary goal is to find creative ways to collect more data more rapidly at more volcanoes. One straightforward way to do this is to relax the previously agreed upon limit of 30 EDS scenes each per month from the United States and Japan, which represents only approximately 0.33% of the average ASTER volume collected in a given month. This requirement has been a long-standing political agreement since the start of the mission and was not developed based on instrument or data limitations. However, it does require increased man-hours for the scheduling process, which

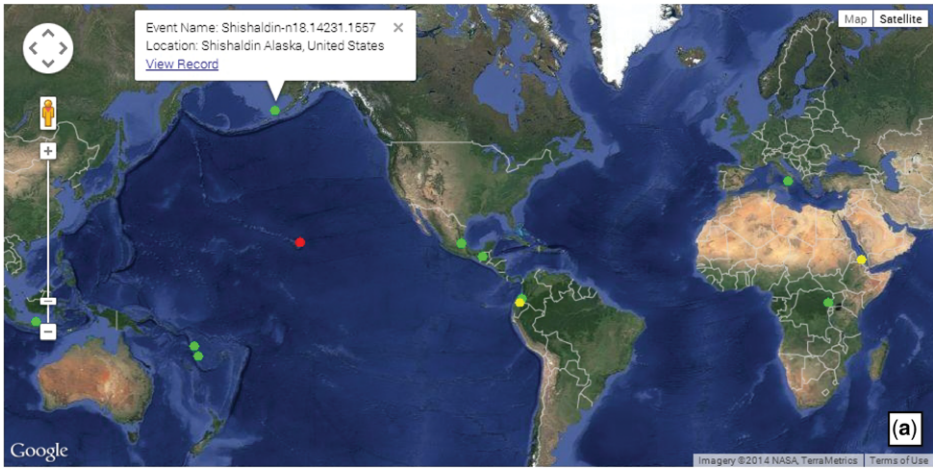

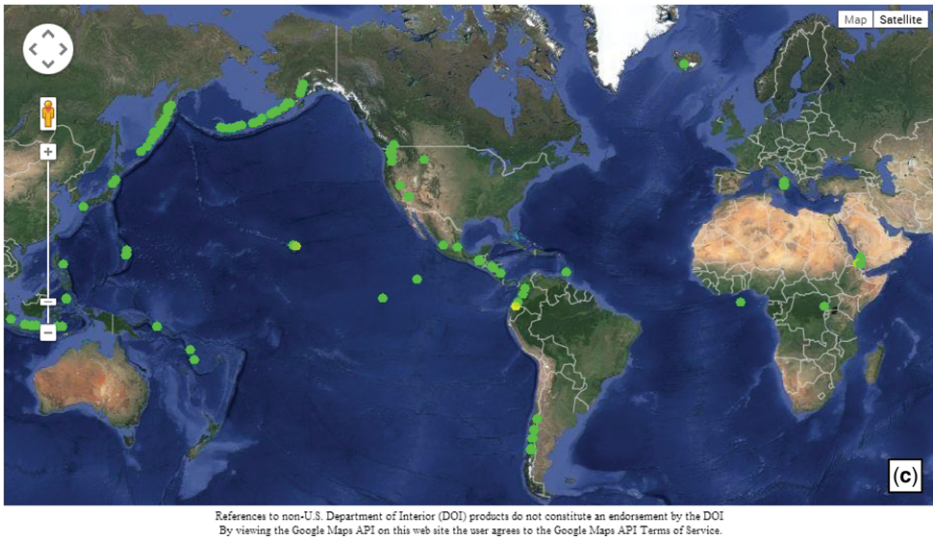

References to non-U.S. Department of Interior (DOI) products do not constitute an endorsement by the DOI
By viewing the Google Maps API on this web site the user agrees to the Google Maps API Terms of Service.

New Approved Completed View All

becomes an impact on available funding. An increase in the number of expedited scenes coming from the URP Program will also result in a small reduction in the total number of scenes acquired elsewhere during any given orbit in ASTER's nominal operational mode. These considerations must be balanced to ensure the continued success of all programmes and agencies relying on ASTER data. It should be noted that there is precedent for increasing the 30 scene per month limit. Figure 2 shows the number of expedited scenes acquired since 2004 and on many occasions the 30 scene per month limit is, in fact, exceeded, nearly doubling on three occasions. However, the 10 year monthly average of expedited scenes is 33.5, only slightly above the limit.

A second approach to improving the number of successfully acquired URP data is to remove and modify the 10 day inhibit window between new triggering requests at a particular volcano. This window was implemented to both limit the amount of traffic coming into the scheduling system and to provide time for the request to be created, uploaded to the sensor and eventually acquired. Typically, this window works well, but on many occasions it has resulted in missed opportunities. The most obvious scenario occurs when the scheduling, the orbital position of Terra and the data acquisition ideally align, and a volcano is observed very quickly after the trigger (in some cases as soon as 24 h). In these cases, there can be 8–9 days of waiting until the inhibit window expires and the next automated trigger is sent, resulting in potential lost observational opportunities. The second scenario is less obvious and results when the opposite case occurs – a situation where scheduling, orbit position and data acquisition do not align and take slightly longer than 10 days. In a worse-case scenario of this situation, the target volcano is scheduled for an observation on day 11 following the triggering event. One day prior to that, however, the 10 day inhibit window expires and a new ASTER URP request is generated. This request then gets rejected because the volcano in question is in the queue for an observation the following day. The 10 day window is then reset at this point and another request is not generated for 9 days following the initial observation. That time combined with the time for scheduling and waiting for the next observation possibility can result in a target being observed as infrequently as every 3 weeks, when it could and should be as frequent as every 10 days (at the equator) and every 1–2 days (at higher latitudes). This issue is being addressed with improvements to both the AESICS system and those systems that monitor the AVHRR and MODIS data. The new scenario removes the 10 day inhibit window completely. All triggering events (as many as 4–6 per day at an active volcano) are streamed directly to the AESICS system, which is now responsible for logging and monitoring the incoming triggers. The first trigger generates an ASTER request (as it does now): subsequent ones, however, do not. During this time, AESICS monitors when the first observation is officially scheduled and when it is completed. Following that, the next trigger from AVHRR or MODIS will spawn a new request immediately. This approach should reduce the time between observations and, therefore, provide more data at all volcanoes. It is currently being tested and expected to be ready for operational implementation by the end of 2015.

Science examples

The role and responsibility of monitoring an eruption and responding to new activity using remote sensing data does not end once an effusive phase transitions to an explosive one or vice versa. For example, eruptive products such as pyroclastic-flow deposits and ash plumes commonly arise either as precursors to effusive activity or as products of that activity. The two are commonly intimately related and understanding one provides insight into the other (e.g. Woods & Koyaguchi 1994; Adams *et al.* 2006). Although some of the following URP science examples do not directly focus on the effusive basaltic eruption theme of this compilation, they do highlight the wide variety of applications made possible by the ASTER URP data and are selected based on that criteria. Furthermore, a fifth example is given in Patrick *et al.* (2015), who focus on the use of TIR data (including ASTER URP data) at the Hawaiian Volcano Observatory (HVO) to monitor the effusive basaltic activity at Kilauea. The first two examples presented here are relevant to effusive eruptions (albeit focused on more evolved lava compositions) in that they examine lava-dome growth and their subsequent collapse to form pyroclastic deposits. The third example

Fig. 2. Google Map interface (part of the AESICS webpage) showing the URP acquisitions over time (Duda *et al.* 2009). **(a)** Recent URP targets over a 2 week period with new requests shown in red, approved/scheduled requests in yellow and acquired data in green. Each target is an active link that displays relevant information and a link to more detailed statistics and the acquired data. **(b)** All URP data acquired from 1 January 2004 to 31 December 2005 during the time period when the URP system operated in a manual-only mode. **(c)** All URP data acquired from the start of the automated URP system (1 January 2006) until 31 August 2014.

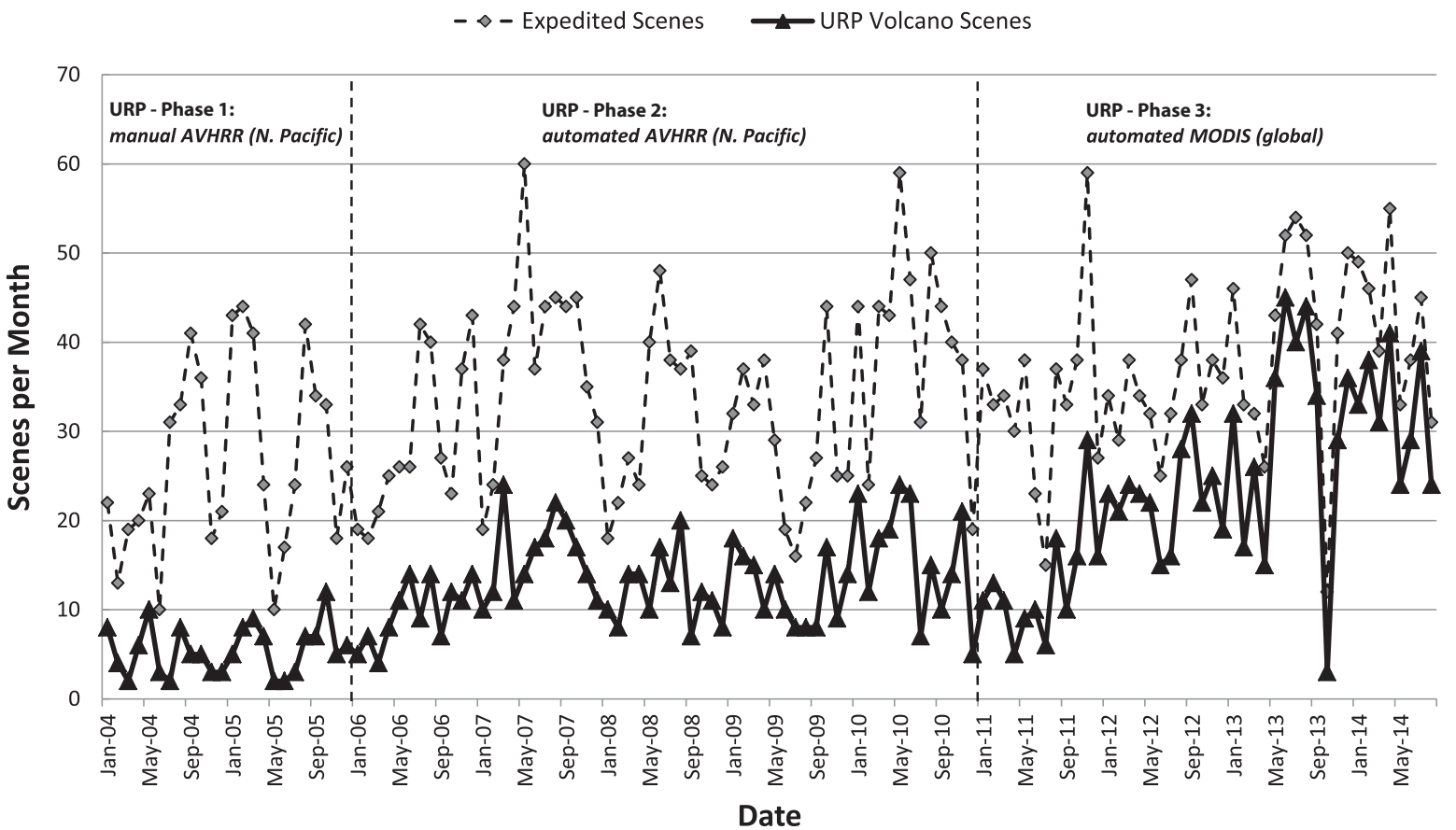

Fig. 3. United States ASTER Science Team expedited scenes (solid line) and URP scenes (dashed line) per month beginning at the start of the URP project in 2004 and showing the three phases of the project. During those phases, the URP data increased from an average of 21.6% to 40.0% to 61.0% of the total expedited data collected by the United States Team, which attests to the success of the URP project.

describes the use of ASTER URP data to map basaltic ash-plume composition following the effusive phase of the eruption, whereas the fourth example is focused directly on monitoring effusive processes. The examples are listed in the order of the development cycle of the URP system (rather than chronologically or on eruption style) from its initial use in a manual-only mode through to its current configuration of automated triggering globally using data from AVHRR and MODIS.

Manual URP science: monitoring ongoing effusive silicic eruption processes. Not every URP trigger event occurs automatically, in which case manual intervention into the EDS is required. A manual triggering interface was the first developed for AESICS and still allows targets to be entered that: (1) show signs of unrest prior to any detectable thermal change; (2) are not included in the list of volcanoes monitored by AVHRR or MODIS; (3) are important field-campaign targets; and/or (4) are not volcano-related disasters and hence have no thermal triggers.

An example of the manual triggering of the URP system occurred in 2006 at the start of increased activity at Merapi volcano, Indonesia (Ramsey 2006). The 2006 eruption of Merapi began with increased seismic activity on 19 March and the first reported sighting of 'volcanic material' moving on the surface occurred on 28 April (Global Volcanism Program 2006). By 11 May, the lava was effusing at a near-constant rate, forming a dome in the summit crater. This effusive activity later gave rise to collapsing dome-flow fronts and subsequent pyroclastic-flow deposits on the SW flank of Merapi (Global Volcanism Program 2006). The global URP system using MODVOLC-detected triggers had not yet been implemented and therefore a manual URP campaign was initiated on 21 April 2006 when seismic activity and SO_2 flux both increased dramatically. This heightened period of manual ASTER URP observations lasted for approximately the next 3 months. Prior to the start of URP observations, ASTER observed Merapi (one of the class A targets in the original ASTER Volcano STAR) approximately once every 12 days. During the URP observational period, Merapi was imaged 20 times in 74 days or approximately once every 3.7 days (Fig. 4). The maximum time separation between these observations was 9 days, whereas the minimum was only 12 h. Most notable about this increased frequency was the number of cloud-free scenes, which was also noted by Urai & Pieri (2011). Nearly 85% of the URP observations were free or partially free of clouds, so that the summit and upper slopes of Merapi were visible. This compares to only 48% of clear to partially clear scenes over the lifetime of ASTER observations of Merapi and confirms the increased probability of usable data when satellite observations occur more frequently.

The first ASTER URP scene was a daytime image acquired on 26 April 2006 and showed no thermal anomalies, but did reveal a small steam plume at the summit. The next scene 2 days later was acquired at night on the same day as the first ground-based reports of volcanic material at the surface. The ASTER data revealed a thermal anomaly for the first time in both the TIR wavelength channels and channels 6–9 of the SWIR. Detection in the SWIR wavelength channels confirmed the presence of material with a minimum pixel-integrated temperature of at least 140°C (Urai *et al.* 1999), which is above the saturation level of the TIR data and typically results where active volcanic material is present. It was not until the images acquired on 5 May (a day–night pair) that SWIR-derived pixel-integrated temperatures in excess of 220°C were detected, which were large enough to confirm that active lava was present on the surface (Fig. 5). Observations continued throughout the next 3 months and all new information derived from the data was disseminated to the Indonesian authorities, as well as to the news media.

A synoptic analysis of these temperatures and the area covered by hot material shows that the 2006 Merapi eruption went through three (possibly four) effusive thermal phases: (1) an initial increase lasting for approximately 2 weeks; (2) a period of maximum output lasting for approximately the same length of time; (3) a slowly waning period of approximately 1 month; and (4) a possible renewal of activity beginning after 8 July 2006 (Fig. 5). During phase 1, derived SWIR temperatures were below saturation and the area covered by these hotter temperatures was only several SWIR pixels in area. Phase 2 was the period of maximum thermal output with temperatures in excess of the saturation threshold for ASTER SWIR ($T > 450$°C). This was also the period when the area covered by these higher temperatures grew in excess of 100 000 m^2 (Fig. 4). Pyroclastic-flow deposits were positively identified to the SE and SW of the summit following the 27 May 2006 M6.3 earthquake, which resulted in an increase in activity including lava-dome growth and numerous pyroclastic-flow-forming collapse events (Global Volcanism Program 2006). Throughout the month of June, both the maximum detected temperature and area covered by hot material slowly declined (phase 3). However, it was during this period (14 June) that the largest pyroclastic flow occurred, which lasted for 3.5 h, produced a deposit to the SE along the Gendol River and killed two people (Global Volcanism Program 2006). The ASTER TIR data acquired on the evening of 15 June clearly detected this deposit and confirmed the estimated

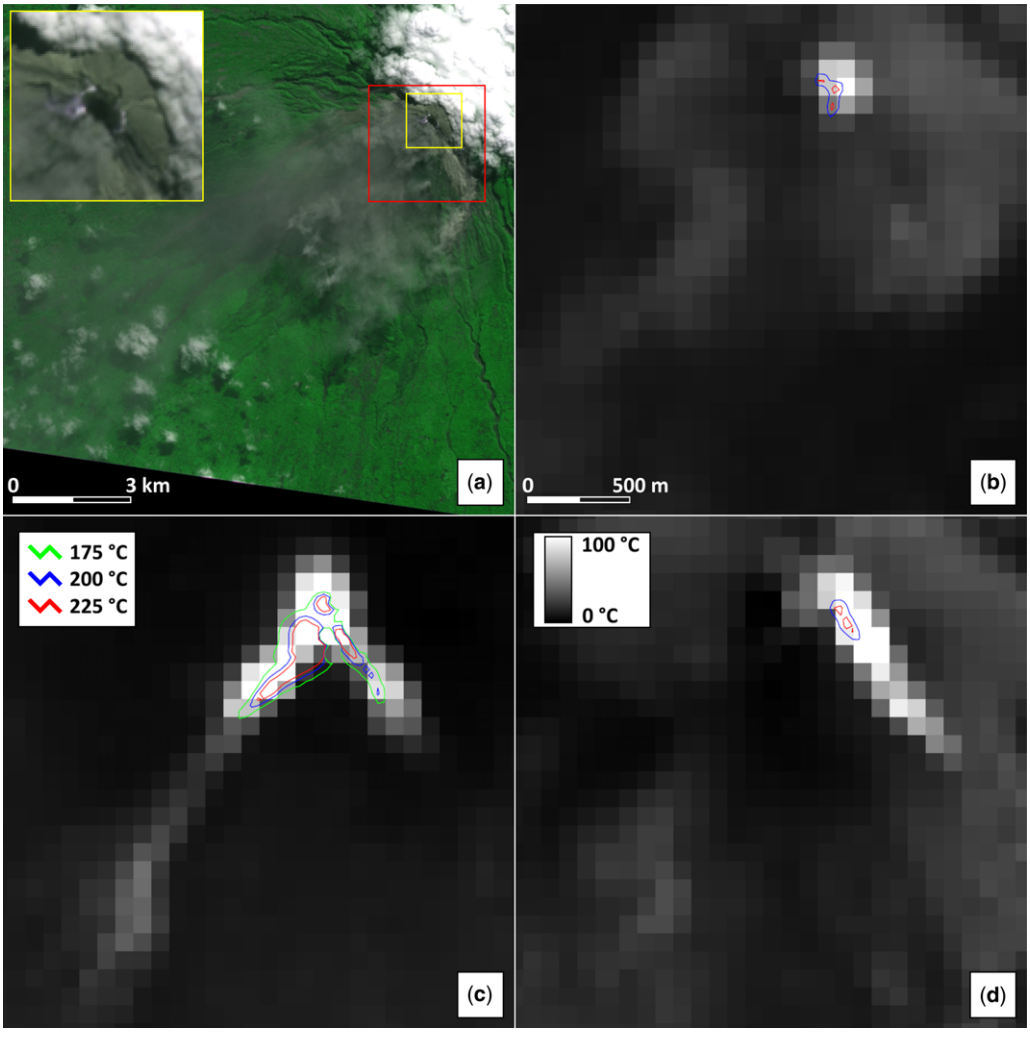

Fig. 4. Examples of the ASTER data acquired at Merapi throughout the 3 month URP observational period in 2006. **(a)** VNIR false-colour image acquired on 6 June at 09:58:54 (local time) with bands 2, 3 and 1 in red, green and blue, respectively. The image captured an ash-rich plume drifting to the SW and fresh pyroclastic-flow deposits to the SE of the summit. The yellow box indicates the area shown in the inset, which is the summit at full spatial resolution, whereas the red box indicates the area shown in the three remaining figures. All figures shown in (b) & (c) are TIR data scaled to the same limits and overlain with colour contours of the SWIR-derived temperatures. Each image was chosen as it was the last acquired in each of the first three phases of the eruption. **(b)** ASTER TIR image acquired on 12 May at 10:05:01 (local time) showing a summit thermal anomaly and the early detection of a SWIR thermal anomaly. **(c)** ASTER TIR image acquired on 30 May at 22:10:13 (local time) showing a very large summit thermal anomaly and the two directions of the pyroclastic-flow deposits. **(d)** ASTER TIR image acquired on 8 July at 09:59:10 (local time) showing the weaker/cooling pyroclastic-flow direction to the SE and a smaller SWIR thermal anomaly.

length of 7.1 km. The decline in thermal output detected by ASTER abruptly reversed on 8 July in the 12 h between the day and night image (Fig. 5). However, throughout the first week of July, the reported activity from ground-based observations decreased and the alert level was lowered. The detected increase in the thermally elevated area in the ASTER data could either signal the last phase of effusive activity at the summit or simply be the result of a very recently emplaced smaller pyroclastic-flow deposit. The 8 July image was the last ASTER URP scene acquired and therefore

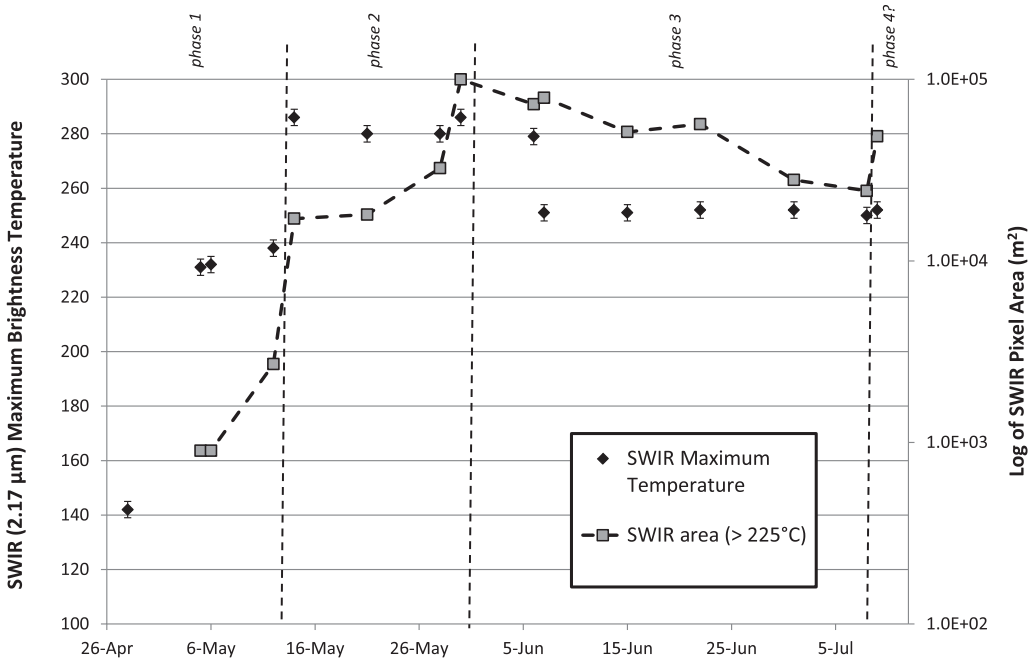

Fig. 5. Time-series graph of the maximum SWIR-derived temperature and surface area covered by temperatures in excess of 225°C. The error bars on the detected temperature correspond to the average reported error for high-temperature SWIR data (±6°C). The error on area is less than the size of the square for each measurement. The phases of activity based on these temperatures and areas are also shown. Phase 1 corresponds to a period of increasing thermal output; phase 2 is the period of maximum thermal output and saturated SWIR temperatures; phase 3 corresponds to decline in thermal output and area; whereas phase 4 may indicate a reverse of that trend.

no further analysis was possible. Although small eruption clouds and pyroclastic-flow deposits were reported throughout July and August, the decrease in activity level early in July formally ended the ASTER URP observational period. The results and near-real time reporting of this eruption using the ASTER data proved to be one of the most successful and well-reported events in the URP Program.

Automated URP science: mapping flow-deposit temperatures as an insight into effusive activity. The initial automated phase of the URP system relied on thermal anomaly triggers from AVHRR data using the UAF system. Testing of this phase started in 2004 and has been operational since 2005, resulting in hundreds of ASTER scenes of volcanic activity in Kamchatka and the Aleutian Arc (e.g. Carter & Ramsey 2010; Rose & Ramsey 2009; Wessels *et al.* 2010; Ramsey *et al.* 2012). One example of the science that resulted from these datasets was the 9 May 2004 eruption of Shiveluch volcano, Kamchatka Peninsula, Russia.

Shiveluch is one of the largest and most active andesitic volcanoes of the Kuril–Kamchatka arc. It commonly alternates between vulcanian explosive eruptions and periods of dome growth that commonly produce subsequent dome-collapse-driven block and ash flows. Explosive activity here is commonly a prelude to subsequent effusive events (Melekestsev *et al*. 1991). Within the last 10 000 years at least 13 large plinian eruptions have occurred, producing distinct and very large debris avalanche deposits to the south (Belousov *et al.* 1999). The May 2004 eruption followed a period of seismic unrest and began with a series of strong ash explosions at the lava dome (Global Volcanism Program 2004). The eruption also produced pyroclastic-flow deposits (PFD), lahar and block/ash flows (BAF), 8–11 km-high ash columns, as well as changes to the lava dome. Scientists from the Russian Institute of Volcanology and Seismology (IVS) found evidence of both pyroclastic and block/ash flows on the south flank of the volcano when they visited 2 weeks later (O. Girina pers. comm.).

The explosive events at Shiveluch are typically the trigger for the URP system and therefore tracking this activity allows the later effusive eruptions to be completely observed. The May 2004 activity resulted in detectable thermal anomalies in

AVHRR that triggered one of the first automated requests of the new ASTER URP system. There were six ASTER observational attempts that month, with the first coming only 2 days after the first URP trigger. ASTER images were acquired on 11 May (night), 20 May (night), 21 May (day), 28 May (day), 30 May (day) and 4 June (day), with all but the 28 and 30 May scenes being clear. The 4 June image was completely cloud-free and the first image acquired following the field-based investigation of the flow deposits. The ASTER data proved valuable for identifying the new deposits, calculating the energy for emplacement and monitoring its cooling over the next 6 months. The multispectral capability of the TIR data also allowed for compositional and textural mapping by way of emissivity variations using the approach of Ramsey & Fink (1999). Greater amounts of surface vesicularity or micron-scale roughness elements on the newly emplaced deposit result in a reduction in the emissivity, which, together with temperature, controls the overall emitted radiance from the surface. This emissivity variation was mapped and the modelled vesicularity found to decrease away from the edges of the lowermost deposit (Fig. 6). This change is visible on field photographs as a darker deposit with more blocks lying stratigraphically above a lighter PFD. The vesicularity mapping points to either a change in block size and density within one depositional event or, more likely, a second BAF deposit perhaps due to partial dome collapse that followed the PFD. Results using the ASTER TIR data for its spectral rather than its temperature information can be applied to many different effusive and explosive flow deposits over the period of an eruption as a means of inferring eruption style and emplacement mechanisms.

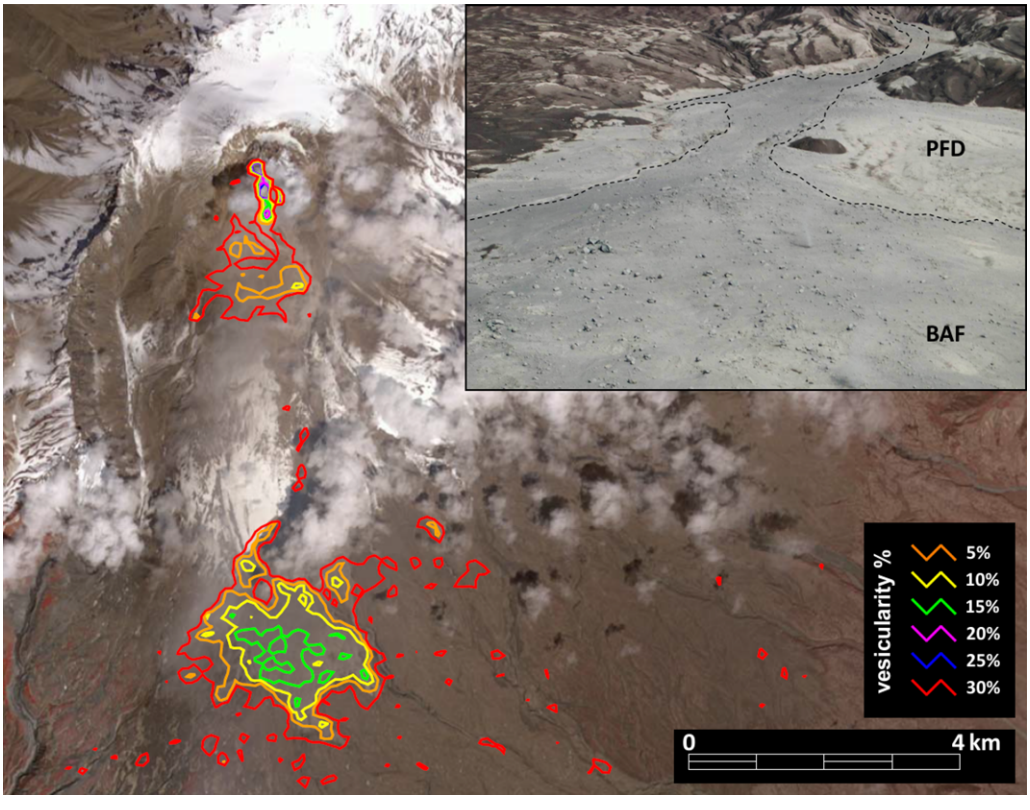

Fig. 6. Flow-deposit mapping on Shiveluch volcano (Kamchatka, Russia) using ASTER URP data collected in the early phase of the automated programme. ASTER VNIR image (base) acquired on 4 June 2004 at 13:37:59 (local time) is overlain with vesicularity contours derived from the TIR emissivity data collected at the same time using the approach of Ramsey & Fink (1999). A small column collapse produced the initial pyroclastic-flow deposit (PDF) followed by a partial dome collapse that formed the block and ash flow (BAF) deposit (see the annotated inset: photograph by O. Girina). The less vesicular BAF deposit is resolved in green in the centre of the lowermost set of closed contours.

Automated URP science: analysis of plume composition following the transition from effusive to explosive activity. Volcanic ash particles are suggested to play a role in perturbing long-wave radiative forcing soon after an eruption (Robock 2000; Neimeier *et al.* 2009). With the possible exception of very large explosive eruptions, any radiative effects of ash are expected to be short-lived, however, as ash is removed from the atmosphere quickly. Nonetheless, these affects are not routinely modelled and thus are poorly constrained (IPCC 2007). Ash can also produce a multitude of other effects such as health hazards to nearby populations (e.g. Delmelle *et al.* 2002; Horwell *et al.* 2010) and danger to aircraft operations (e.g. Hufford *et al.* 2000; Prata & Tupper 2009). The presence of volcanic ash in a plume can generally be detected using the TIR 'split window' approach of Prata (1989) applied to a suite of satellite sensor data (e.g. MODIS, AVHRR), with a few well-known limitations (e.g. Simpson *et al.* 2000, 2001; Prata *et al.* 2001). Higher spectral resolution TIR data from sensors such as Atmospheric Infrared Sounder (AIRS) and Infrared Atmospheric Sounding Interferometer (IASI) provide more compositional information and eliminate the need for the split window approach (Carn *et al.* 2005; Karagulian *et al.* 2010; Prata *et al.* 2010). However, a detailed plume analysis from space using these sensors is limited by their much low spatial resolution. Therefore, lacking is the compositional analysis of the nascent/proximal portion of the plume at a higher spatial resolution. This proximal region is a complex and dynamic mixture of varying particle sizes from 0.1 to 100 μm (Piscini *et al.* 2011), possible compositions and varying temperatures. The concentrations of these products will also change temporally and spatially over short distances, and therefore can relate directly to the eruptive process and vent dynamics.

During the 2010 effusive activity at Fimmvörðuháls, Iceland, automated URP data, initially triggered by the MODVOLC system, were examined. This activity was ongoing prior to the explosive eruption at Eyjafjallajökull. In contrast to the prior example at Shiveluch, effusive activity at Fimmvörðuháls was the prelude to the subsequent explosive activity. However, similar to Shiveluch, explosive and effusive activity are related, and therefore orbital data acquired throughout the entirety of an eruption provide important information (e.g. Harris *et al.* 1997*b*; Wright *et al.* 2005). Here, the focus is on the analysis of the TIR data later acquired over one of the ash plumes produced by Eyjafjallajökull. Emissivity was extracted from the ASTER TIR data, with particular attention paid to the plume rather than the surface deposits. However, rather than mapping micron-scale texture as was done at Shiveluch in 2004, a library of fine-grained mineral and glass spectra was used to map the compositional variability in the plume (Fig. 7), with the assumption that the proximal plume emits as an opaque solid surface. The spectral library mapping approach was developed by Ramsey & Christensen (1998) using a linear deconvolution technique to map the fraction of each library end member in every pixel in order to produce end-member compositional maps. This modelling approach had not been used on active plumes and is valid only for the proximal plume, which is more dense and much warmer than the surrounding atmosphere. Proper understanding of emission theory and the use of the correct end members allowed this model to be applied in such a case, and results in the 5–10 μm andesite glass being the best fit to the ash-rich plume. Work is ongoing to constrain the range of possible library end members and size fractions, collect spectral data of airborne ash in the laboratory, and apply the approach to other plumes in the ASTER URP archive (Williams & Ramsey 2014).

Automated URP science: calculating lava-flow volumes. A more recent application of the automated URP data triggered by AVHRR is the 2012–13 eruption of Tolbachik volcano, Kamchatka Peninsula, Russia. The eruption that began in November 2012 is the first effusive activity at Tolbachik since the 'Great Tolbachik Fissure Eruption', which started on 6 July 1975 and ended 17 months later (Fedotov *et al.* 1991). The number of shallow volcanic earthquakes increased on 26 November 2012 and observers from the village of Kozyrevsk (50 km to the NW) reported ash explosions and new lava flows (Global Volcanism Program 2012). Basaltic lava effused from two fissures and a very large thermal anomaly was detected by the AVHRR sensor, which immediately triggered the URP system. Vigorous strombolian fire-fountaining activity continued and fast-moving open-channel lava flows quickly formed. Over the first few months of 2013, the eruption continued and changes to local topography from the cooling flows resulted in new flow directions that propagated to the east of the fissure system, slowly building up a complex flow field (Fig. 8).

By the time of the first clear ASTER night-time data acquisition on 2 December 2012, two flows were visible: the larger flow measured 9.7 km in length (Fig. 8a). The smaller flow (5.5 km long) had already stopped and was cooling in this image. With the next several ASTER datasets, the larger flow grew to a length of 13.5 km some 13 h later (ASTER daytime image) and to 17 km by 8 December, with numerous smaller breakouts and visible flow-pirating of the central channel by newer flows. The average advance rate of the larger

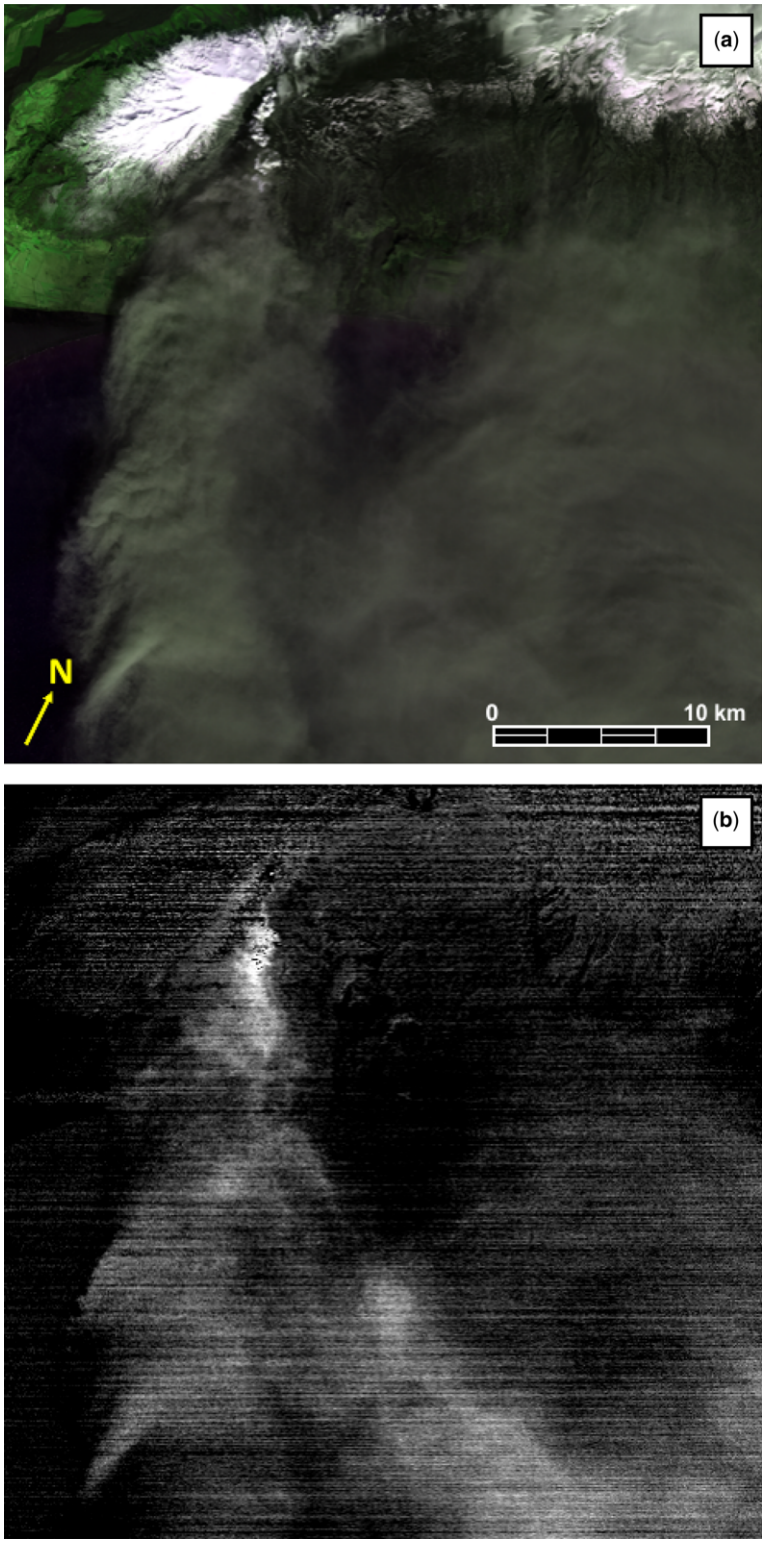

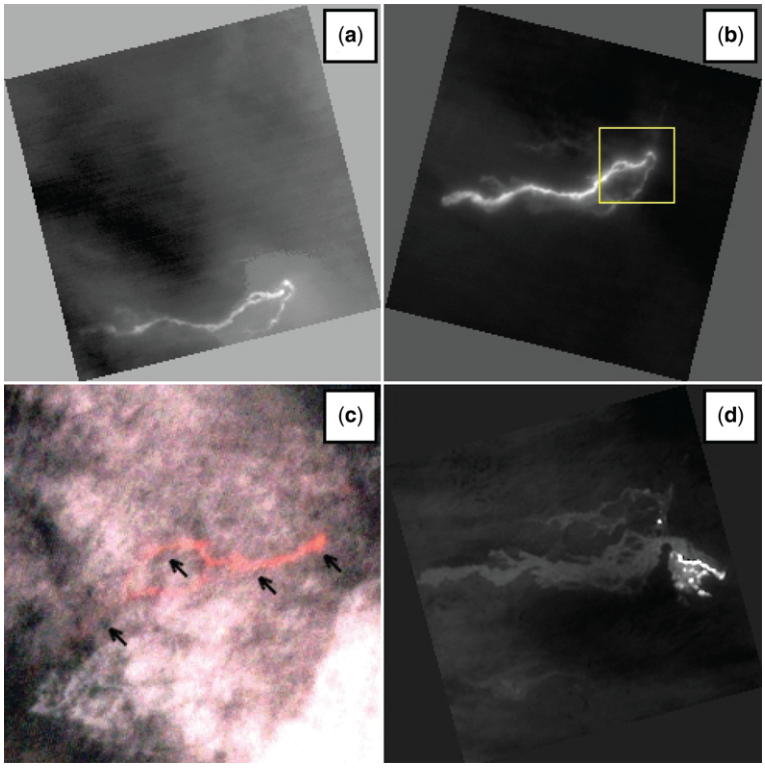

Fig. 8. Examples of ASTER URP data for the 2012–13 Tolbachik eruption. **(a)** The first clear night-time TIR URP image acquired on 2 December 2012 at 23:08:39 (local time). Moderate cloud cover was present: however, two vents and flows are visible. **(b)** Daytime TIR image acquired nearly 13.5 h after (a) with slightly less cloud cover. The yellow box indicates the area shown in (c). **(c)** VNIR image collected at the same time as (b) showing the incandescent flow (denoted by black arrows) through heavier cloud cover. **(d)** Night-time TIR image acquired on 5 Jun 2013 at 23:02:53 (local time) near the end of the extrusive phase. A thin cloud area is also present: however, the entire cooling flow field can be seen, as well as the active vent and the most recent open channel feeding the SE flow field. Each image shown in (a), (b) & (d) are 18 × 18 km and all images are orientated with north up.

flow was calculated from these length measurements, changing from 0.08 to 0.04 m s^{-1} over the period between 26 November and 8 December.

During the first 6 months of 2013, the eruption was continually observed by ASTER, and changes in activity and flow area were documented. The activity continued less vigorously over this time, with the exception of several pulses of higher activity. The flow area containing TIR thermally elevated pixels (i.e. those $>5^{\circ}C$ above the average background temperature) and covering a new area from the previous scene was measured over this time period (Fig. 9). By June 2013, the maximum area of the entire flow field was slightly greater than 37 km^2. The flow volume and effusion rate were derived from these area measurements, and by either assuming or measuring the thickness of each new flow. The ASTER DEMs generated from the VNIR data were used to estimate changes in flow thickness. The DEMs were only marginally successful as the vertical error in the DEM is at or near the flow thickness for all but the largest flows. Furthermore, the DEMs are not available for the night-time images as no VNIR data are acquired. Therefore, an assumed average thickness of 3.0 m was used in these cases (Fig. 9). With the exception of the initial phase and two large pulses in February and April, the average effusion rate for the entire eruption was 4.9 m^3 s^{-1}. This rate increased to approximately 150 m^3 s^{-1} during the larger effusive

Fig. 7. ASTER URP data acquired on 19 April 2010 at 12:51:31 (local time) of the ongoing Eyjafjallajökull (Iceland) eruption showing the proximal plume. **(a)** VNIR false colour image. **(b)** Linear spectral deconvolution result varying from approximately 80% concentration (white) to 0% (black) for a 5 μm andesitic glass end member.

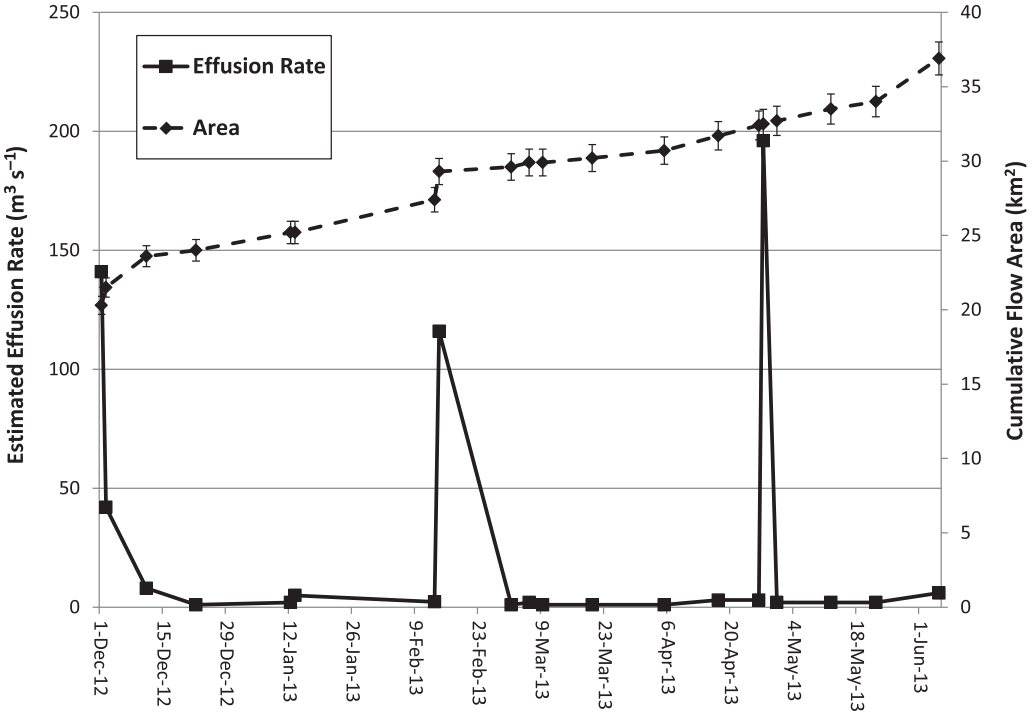

Fig. 9. Cumulative flow area and effusion rate of the 2012–13 Tolbachik eruption calculated from ASTER URP data. The flow area was measured in each image, with care taken to only map thermally elevated pixels covering new areas. Errors bars represent a 4% pixel measurement uncertainty arising from the possibility of counting pixels that do not contain active lava. This 'thermal bleed over' effect can occur as a result of the ASTER instantaneous field of view (IFOV) causing high-temperature pixels to artificially 'illuminate' cooler adjacent pixels, which then appear to be thermally elevated (Rose *et al.* 2014). The effusion rate was calculated using ASTER-derived DEMs to estimate flow thickness, as well as assuming a constant average value of 3.0 m based on field observations.

phases. The maximum atmospherically corrected, pixel-integrated brightness temperature was commonly near or slightly above 100°C for regions of pixels in most ASTER TIR scenes over the first 6 months of the eruption. This is at the saturation level of the TIR data and typically results where open-channel basalt flows are occurring, which was validated during field observations by Russian scientists. Therefore, results from this study show that the evolution of a large effusive flow field over time can be documented using measurements of the day and night temperature from ASTER TIR data and the flow thickness from the ASTER VNIR data. Similar approaches can easily be applied to the flow fields of, for example, the Kilauea, Etna or Piton de la Fournaise volcanoes.

Conclusions

Monitoring of active volcanic processes using spaceborne data commonly requires different temporal, spatial and spectral scales depending on the science goal and the process being observed. However, there is not one system currently in operation that collects data at the ideal scale for every application. High temporal–low spatial resolution is ideal for the study of transient processes and has been used quite effectively in the past to translate remote sensing data such as thermal emission into volcanological data such as effusion rates (e.g. Harris *et al.* 1997*a*, 1999). This scale is also ideal for detecting new activity provided that it is extensive and/or thermally elevated enough to be resolved in 1 km (or larger) pixels. High spatial–low temporal resolution lies on the other end of the monitoring spectrum in that it provides image-based information near/at the scale of ground-based observations. These images are important for validation of the lower spatial resolution data, as well as for the interpretation of smaller-scale processes such as the temperature of a growing lava dome, the shape/length of an advancing flow or the assessment of damage following an eruption. Neither class of sensor

provides all the information required for assessing an eruption completely, and therefore both should be used synergistically where practical.

The ASTER URP system was implemented in 2004 as way to provide this synergistic monitoring and scientific analysis for new volcanic eruptions. It takes advantage of both the scheduled nature of ASTER and the provision for rapid acquisition and processing, known as the expedited data system. The URP also relies on previously established monitoring programmes using AVHRR data in the North Pacific region and MODIS data globally to trigger the EDS pathway and acquire new ASTER observations semi-automatically anywhere from 1 to 7 days following the trigger. The current average time is approximately 4 days, depending on the latitude of the volcano and the position of the spacecraft at the time of the request. This heightened observational schedule continues throughout the period of eruption as long as the AVHRR and MODIS sensors are able to detect elevated thermal output. The URP system has thus far evolved through three phases of development and now acquires a new volcanic image every 1.3 days, on average, with over 2000 volcano-specific datasets in the archive. With new funding from NASA and the continued operation of ASTER, the system should continue to operate until at least 2017, making the URP one of the longest, continually funded NASA programmes focused on both mission operations and volcanic science. The current phase 4 of the programme will improve the response time further, as well as acquire more images per month at more volcanoes globally.

The ever-expanding URP archive is now being used to examine past eruptions to extract important monitoring queues, as well as retrospectively for numerous scientific applications. For example, the combined use of the VNIR and TIR collected in two scenes within 12 h of each other provides a means to derive thermal inertia, the thermophysical parameter that can be modelled to extract particle and block size, as well as determine mantling thicknesses of pyroclastic airfall deposits. This approach has applications for both terrestrial volcanic and planetary aeolian processes. Moderate spatial scale TIR data with more than one–three spectral channels are unique to ASTER, and provide the ability to extract both temperature and emissivity from the radiance data. Emissivity can be modelled to derive the composition of the deposit or potentially the proximal ash-rich plume, as shown for the 2010 eruption of Eyjafjallajökull. The same emissivity is also sensitive to roughness at the micron-scale, allowing surface vesicularity to be extracted and thereby determine eruption/emplacement mechanisms, as shown for the 2004 eruption of Shiveluch. Finally, the 90 m/pixel TIR data processed into ground-based temperature is ideally suited for mapping lava-flow changes and advance rates over time. This approach is easily automated to extract parameters such as flow advance rate, aerial coverage, and volume and effusion rates, as shown for both the 2006 eruption of Merapi and the 2012 eruption of Tolbachik.

Finally, the URP archive has also provided a unique resource for new mission planning. The future NASA Hyperspectral Infrared Imager (HyspIRI) mission, for example, is scheduled to have a multispectral TIR imager similar to ASTER but with several important improvements. The HyspIRI TIR system will have a 5 day temporal coverage at the equator (1 day at higher latitudes), with several more spectral channels including a high-temperature channel in the 3–5 μm region. Because ASTER URP data are commonly acquired near this temporal resolution, they provide a unique archive to estimate factors such as expected cloud coverage and the predicted surface change expected to been seen in HyspIRI data (Ramsey *et al.* 2013). Furthermore, the rare VNIR data acquired at night with ASTER allowed determination of the high-temperature saturation threshold for HyspIRI (Realmuto *et al.* 2011). All of these TIR-based scientific studies rely on continued acquisition of well-calibrated operational TIR data from ASTER, rigorous field and laboratory-based research and validation, and the participation of groups in academia and government to maintain the current monitoring programmes and operational systems, and to utilize the higher-resolution data.

Funding for this research project was made possible through the NASA Science of Terra and Aqua Program (grant numbers: NNG04GO69G, NNX08AJ91G, NNX11AL29G, NNX14AQ96G). The author would like to thank the many URP investigators, collaborators and students that have devoted their time and skills to the project over the years, including: S. Belousov, M. Belousov, A. Carter, J. Dehn, K. Duda, O. Girina, A. Harris, T. Hughes, J. Krippner, L. Maldonado, H. Morgan, M. Patrick, E. Pilger, S. Rose, K. Reath, A. Steffke, M. Watson, R. Wessels, D. Williams and R. Wright. This manuscript was greatly improved by the detailed and helpful reviews of D. Pieri and S. Carn.

References

Adams, N. K., Houghton, B. F. & Hildreth, W. 2006. Abrupt transitions during sustained explosive eruptions: examples from the 1912 eruption of Novarupta, Alaska. *Bulletin of Volcanology*, **69**, 189–206.

Belousov, A., Belousova, M. & Voight, B. 1999. Multiple edifice failures, debris avalanches and associated eruptions in the Holocene history of Shiveluch volcano, Kamchatka, Russia. *Bulletin of Volcanology*, **61**, 324–342.

Carn, S., Strow, L., DeSouza-Machado, S., Edmonds, Y. & Hannon, S. 2005. Quantifying tropospheric

volcanic eruptions with AIRS: the 2002 eruption of Mt. Etna (Italy). *Geophysical Research Letters*, **32**, L02301, http://doi.org/10.1029/2004GL021034

Carter, A. J. & Ramsey, M. S. 2010. Long-term volcanic activity at Shiveluch Volcano: nine years of ASTER spaceborne thermal infrared observations. *Remote Sensing*, **2**, 2571–2583, http://doi.org/10.3390/rs2112571

Carter, A. J., Ramsey, M. S. & Belousov, A. B. 2007. Detection of a new summit crater on Bezymianny Volcano lava dome: satellite and field-based thermal data. *Bulletin of Volcanology*, **69**, 811–815, http://doi.org/10.1007/s00445-007-0113-x

Davies, A. G., Chien, S., Tran, D. & Doubleday, J. 2015. The NASA Volcano Sensor Web, advanced autonomy and the remote sensing of volcanic eruptions: a review. *In*: Harris, A., De Groeve, T., Garel, F. & Carn, S. A. (eds) *Detecting, Modelling and Responding to Effusive Eruptions*. Geological Society, London, Special Publications, **426**. First published online June 22, 2015, http://doi.org/10.1144/SP426.3

Dean, K. G., Servilla, M., Roach, A., Foster, B. & Engle, K. 1998. Satellite monitoring of remote volcanoes improves study efforts in Alaska. *Eos, Transactions of the American Geophysical Union*, **79**, 413–423.

Dehn, J., Dean, K. & Engle, K. 2000. Thermal monitoring of North Pacific volcanoes from space. *Geology*, **28**, 755–758.

Delmelle, P., Stix, J., Baxter, P., Garcia-Alvarez, J. & Barquero, J. 2002. Atmospheric dispersion, environmental effects and potential health hazard associated with the low altitude gas plume of Masaya volcano, Nicaragua. *Bulletin of Volcanology*, **64**, 423–434.

Duda, K. A. 2012. NASA and USGS ASTER expedited satellite data services for disaster situations. *In*: *American Geophysical Union, Fall Meeting 2012*, San Francisco, CA, 3–7 December 2012. American Geophysical Union, Washington, DC, Abstract IN33C-1548.

Duda, K. A. & Abrams, M. 2012. ASTER Satellite observations for international disaster management. *Proceedings of the IEEE*, **100**, 2798–2811.

Duda, K. A., Ramsey, M., Wessels, R. & Dehn, J. 2009. Optical satellite volcano monitoring: a multi-sensor rapid response system. *In*: Ho, P. P. (ed.) *Geoscience and Remote Sensing*. INTECH Press, Vukovar, Croatia, 473–496.

Fedotov, S. A., Balesta, S. T., Dvigalo, V. N., Razina, A. A., Flerov, G. B. & Chirkov, A. M. 1991. New Tolbachik volcanoes, Chapter 10. *In*: Fedotov, S. A. & Masurenkov, Yu. P. (eds) *Active Volcanoes of Kamchatka*, Volume 1. Nauka, Moscow, 214–279.

Flynn, L. P., Wright, R., Garbeil, H., Harris, A. J. & Pilger, E. 2002. A global thermal alert system using MODIS: initial results from 2000 to 2001. *Advances in Environmental Monitoring and Modelling*, **1**, 37–69.

Friedman, J. D. & Williams, R. S. 1970. Changing patterns of thermal emission from Surtsey, Iceland, between 1966 and 1969. *In*: *Geological Survey Research 1970, Chapter D*. United States Geological Survey, Professional Papers, **700-D**, 116–124.

Ganci, G., Bilotta, G., Cappello, A., Herault, A. & Del Negro, C. 2015. HOTSAT: a multiplatform system for the satellite thermal monitoring of volcanic activity. *In*: Harris, A., De Groeve, T., Garel, F. & Carn, S. A. (eds) *Detecting, Modelling and Responding to Effusive Eruptions*. Geological Society, London, Special Publications, **426**. First published online October 29, 2015, http://doi.org/10.1144/SP426.21

Gawarecki, S. J., Lyon, R. J. P. & Nordberg, W. 1965. Infrared spectral returns and imagery of the Earth from space and their application to geological problems. *In*: Badgley, P. C. (ed.) *Scientific Experiments for Manned Orbital Flight*. American Astronautical Society, Science and Technology Series, **4**, 13–133.

Global Volcanism Program 2004. Report on Sheveluch (Russia). *In*: Wunderman, R. (ed.) *Bulletin of the Global Volcanism Network*, **29**, (5). Smithsonian Institution, Washington, DC, http://doi.org/10.5479/si.GVP.BGVN200405-300270

Global Volcanism Program 2006. Report on Merapi (Indonesia). *In*: Wunderman, R. (ed.) *Bulletin of the Global Volcanism Network*, **31**, (5). Smithsonian Institution, Washington, DC, http://doi.org/10.5479/si.GVP.BGVN200605-263250

Global Volcanism Program 2012. Report on Tolbachik (Russia). *In*: Wunderman, R. (ed.) *Bulletin of the Global Volcanism Network*, **37**, (12). Smithsonian Institution, Washington, DC, http://doi.org/10.5479/si.GVP.BGVN201212-300240

Harris, A. J. L., Blake, S., Rothery, D. A. & Stevens, N. F. 1997*a*. A chronology of the 1991 to 1993 Etna eruption using AVHRR data: implications for real time thermal volcano monitoring. *Journal of Geophysical Research*, **102**, 7985–8003.

Harris, A. J. L., Keszthelyi, L. *et al.* 1997*b*. Chronology of the episode 54 eruption at Kilauea volcano, Hawaii, from GOES-9 satellite data. *Geophysical Research Letters*, **24**, 3281–3284.

Harris, A. J. L., Flynn, L. P., Rothery, D. A., Oppenheimer, C. & Sherman, S. B. 1999. Mass flux measurements at active lava lakes: implications for magma recycling. *Journal of Geophysical Research*, **104**, 7117–7136.

Hirn, B., Di Bartola, C., Laneve, G., Cadau, E. & Ferrucci, F. 2008. SEVIRI onboard Meteosat Second Generation, and the quantitative monitoring of effusive volcanoes in Europe and Africa. *In*: *Geoscience and Remote Sensing Symposium, 2008 IEEE International-IGARSS 2008*, Boston, Massachusetts, USA, 4–11 July 2008. IEEE (Institute of Electrical and Electronics Engineers), Piscataway, NJ, III-374–III-377.

Horwell, C. J., Le Blond, J. S., Michnowicz, S. A. K. & Cressey, G. 2010. Cristobalite in a rhyolitic lava dome: evolution of an ash hazard. *Bulletin of Volcanology*, **72**, 249–253.

Hufford, G., Simpson, J. J., Salinas, L., Barske, E. & Pieri, D. C. 2000. Operational considerations of volcanic ash for airlines. *Bulletin of the American Meteorological Society*, **8**, 745–755.

IPCC 2007. *Climate Change 2007: The Physical Science Basis. Contribution of Working Group I to the Fourth Assessment Report of the Intergovernmental Panel on Climate Change*. Solomon, S., Qin, D. *et al.* (eds) Cambridge University Press, Cambridge, UK.

KAHLE, A. B., PALLUCONI, F. D., HOOK, S. J., REALMUTO, V. J. & BOTHWELL, G. 1991. The advanced spaceborne thermal emission and reflectance radiometer (ASTER). *International Journal of Imaging System Technology*, **3**, 144–156.

KARAGULIAN, F., CLARISSE, L., CLERBAUX, C., PRATA, A. J., HURTMANS, D. & COHEUR, P. F. 2010. Detection of volcanic SO_2, ash, and H_2SO_4 using the infrared atmospheric sounding interferometer (IASI). *Journal of Geophysical Research*, **115**, D00L02, http://doi.org/10.1029/2009JD012786

MELEKESTSEV, I. V., VOLYNETS, O. N., YERMAKOV, V. A., KIRSANOVA, T. P. & MASUREKOV, Yu. P. 1991. New Tolbachik Volcanoes, Chapter 5. *In*: FEDOTOV, S. A. & MASURENKOV, Yu. P. (eds) *Active Volcanoes of Kamchatka – Vol. 1*. Nauka Publishers, Moscow, Russia, 82–103.

NEIMEIER, U., TIMMRECK, C., GRAF, H.-F., KINNE, S., RAST, S. & SELF, S. 2009. Initial fate of fine ash and sulfur from large volcanic eruptions. *Atmospheric Chemistry and Physics*, **9**, 9043–9057.

PATRICK, M. R., KAUAHIKAUA, J., DAVIES, A., RAMSEY, M., ANTOLIK, L. & LEE, L. 2015. Operational thermal remote sensing and lava flow monitoring at the Hawaiian Volcano Observatory. *In*: HARRIS, A., DE GROEVE, T., GAREL, F. & CARN, S. A. (eds) *Detecting, Modelling and Responding to Effusive Eruptions*. Geological Society, London, Special Publications, **426**. First published online August 6, 2015, http://doi.org/10.1144/SP426.17

PIERI, D. & ABRAMS, M. 2004. ASTER watches the world's volcanoes: a new paradigm for volcanological observations from orbit. *Journal of Volcanology and Geothermal Research*, **135**, 13–28.

PISCINI, A., CORRADINI, S., MARCHESE, F., MERUCCI, L., PERGOLA, N. & TRAMUTOLI, V. 2011. Volcanic ash cloud detection from space: a comparison between the RSTASH technique and the water vapour corrected BTD procedure. *Geomatics, Natural Hazards and Risk*, **2**, 1–15.

PRATA, A. J. 1989. Observations of volcanic ash clouds in the 10–12 μm window using AVHRR/2 data. *International Journal of Remote Sensing*, **10**, 751–761.

PRATA, A. J. & TUPPER, A. 2009. Aviation hazards from volcanoes: the state of the science. *Natural Hazards*, **51**, 239–244.

PRATA, A. J., GANGALE, G., CLARISSE, L. & KARAGULIAN, F. 2010. Ash and sulfur dioxide in the 2008 eruptions of Okmok and Kasatochi: insights from high spectral resolution satellite measurements. *Journal of Geophysical Research*, **115**, D00L18, http://doi.org/10.1029/2009JD013556

PRATA, F., BLUTH, G., ROSE, W. I., SCHNEIDER, D. & TUPPER, A. 2001. Comments on 'Failures in detecting volcanic ash from a satellite-based technique'. *Remote Sensing of Environment*, **78**, 341–346.

RAMSEY, M. S. 2006. The critical need for moderate to high resolution thermal infrared data for volcanic hazard mitigation and process monitoring from the micron to the kilometer scale. *In*: *American Geophysical Union, Fall Meeting 2006*, San Francisco, CA, 11–15 December 2006. American Geophysical Union, Washington, DC, Abstract H32D-06.

RAMSEY, M. S. & CHRISTENSEN, P. R. 1998. Mineral abundance determination: quantitative deconvolution of thermal emission spectra. *Journal of Geophysical Research*, **103**, 577–596.

RAMSEY, M. S. & DEHN, J. 2004. Spaceborne observations of the 2000 Bezymianny, Kamchatka eruption: the integration of high-resolution ASTER data into near real-time monitoring using AVHRR. *Journal of Volcanology and Geothermal Research*, **135**, 127–146.

RAMSEY, M. S. & FINK, J. H. 1999. Estimating silicic lava vesicularity with thermal remote sensing: a new technique for volcanic mapping and monitoring. *Bulletin of Volcanology*, **61**, 32–39.

RAMSEY, M. S. & FLYNN, L. P. 2004. Strategies, insights, and the recent advances in volcanic monitoring and mapping with data from NASA's Earth Observing System. *Journal of Volcanology and Geothermal Research*, **135**, 1–11.

RAMSEY, M. S. & HARRIS, A. J. L. 2013. Volcanology 2020: how will thermal remote sensing of volcanic surface activity evolve over the next decade? *Journal of Volcanology and Geothermal Research*, **249**, 217–233.

RAMSEY, M. S., DEHN, J., WESSELS, R., BYRNES, J., DUDA, K., MALDONADO, L. & DWYER, J. 2004. The ASTER emergency scheduling system: a new project linking near-real-time satellite monitoring of disasters to the acquisition of high-resolution remote sensing data. *In*: *American Geophysical Union, Fall Meeting 2004*, San Francisco, CA, 13–17 December 2004. American Geophysical Union, Washington, DC, Abstract SF23A-0026.

RAMSEY, M. S., WESSELS, R. L. & ANDERSON, S. W. 2012. Surface textures and dynamics of the 2005 lava dome at Shiveluch Volcano, Kamchatka. *Geological Society of America Bulletin*, **124**, 678–689, http://doi.org/10.1130/B30580.1

RAMSEY, M. S., REATH, K. A. & WILLIAMS, D. B. 2013. Threshold considerations for future volcanic hotspot and ash detection using HyspIRI. *Paper presented at the 2013 HyspIRI Science Workshop*, Pasadena, CA, 15–17 October 2013.

REALMUTO, V., HOOK, S. *ET AL.* 2011. *HyspIRI High-Temperature Saturation Study*. JPL Publication, **11-2**. Jet Propulsion Laboratory, Pasadena, CA.

ROBOCK, A. 2000. Volcanic eruptions and climate. *Reviews of Geophysics*, **38**, 191–219.

ROSE, S. R. & RAMSEY, M. S. 2009. The 2005 eruption of Kliuchevskoi volcano: chronology and processes derived from ASTER spaceborne and field-based data. *Journal of Volcanology and Geothermal Research*, **184**, 367–380.

ROSE, S. R., WATSON, I. M., RAMSEY, M. S. & HUGHES, C. G. 2014. Thermal deconvolution: accurate retrieval of multispectral infrared emissivity from thermally-mixed volcanic surfaces. *Remote Sensing of the Environment*, **140**, 690–703.

SCHEIDT, S., LANCASTER, N. & RAMSEY, M. 2011. Eolian dynamics and sediment mixing in the Gran Desierto, Sonora, MX: fusion of infrared orbital and emission spectroscopy data. *Geological Society of America Bulletin*, **123**, (7–8), 1628, http://doi.org/10.1130/B30338.1

Scorer, R. S. 1986. Etna: the eruption of Christmas 1985 as seen by a meteorological satellite. *Weather*, **41**, 378–384.

Simpson, J. J., Hufford, G., Pieri, D. C. & Berg, J. 2000. Failures in detecting volcanic ash from satellite data. *Remote Sensing of Environment*, **72**, 191–217.

Simpson, J. J., Hufford, G., Pieri, D. C. & Berg, J. 2001. Response to comments on 'Failures in detecting volcanic ash from satellite data'. *Remote Sensing of Environment*, **72**, 191–217.

Steffke, A. M. & Harris, A. J. L. 2010. A review of algorithms for detecting volcanic hot spots in satellite infrared data. *Bulletin of Volcanology*, **73**, 1109–1137.

Urai, M. 2004. Sulfur dioxide flux estimation from volcanoes using advanced spaceborne thermal emission and reflection radiometer: A case study of Miyakejima volcano, Japan. *Journal of Volcanology and Geothermal Research*, **134**, 1–13.

Urai, M. & Pieri, D. C. 2011. ASTER applications in volcanology. *In*: Ramachandran, B., Justice, C. O. & Abrams, M. J. (eds) *Land Remote Sensing and Global Environmental Change: NASA's Earth Observing System and the Science of ASTER and MODIS*. Springer, New York, 245–272, http://doi.org/10.1007/978-1-4419-6749-7

Urai, M., Keiichi, F., Yamaguchi, Y. & Pieri, D. C. 1999. Volcano observation potential and global volcano monitoring plan with ASTER. *Bulletin of the Volcanological Society of Japan*, **44**, 131–141.

Wessels, R. L., Schneider, D. J., Coombs, M. L., Dehn, J. & Ramsey, M. S. 2010. High-resolution satellite and airborne thermal infrared imaging of the 2006 eruption of Augustine Volcano, Alaska. *In*: Power, J. A., Coombs, M. L. & Freymueller, J. T. (eds) *The 2006 Eruption of Augustine Volcano, Alaska.* United States Geological Survey, Professional Papers, **1769**, 527–553.

Williams, R. S. & Friedman, J. D. 1970. Satellite observation of effusive volcanism. *Journal of the British Interplanetary Society*, **23**, 441–450.

Williams, D. B. & Ramsey, M. S. 2014. Analyzing proximal volcanic ash emissions using high spatial resolution thermal infrared imagery. *In*: Bursik, M., Kuehn, S., Pouget, S. & Wallace, K. (eds) *Tephra 2014: Maximizing the Potential of Tephra for Multidisciplinary Science*, 100–101, https://vhub.org/resources/3283

Wilson, R. A., Dehn, J., Prakash, A. & Wessels, R. 2007. Lava effusion rates from satellite remote sensing for Kliuchevskoi volcano, Kamchatka–Russia in 2007. *In*: *American Geophysical Union, Fall Meeting 2007*, San Francisco, CA, 10–14 December 2004. American Geophysical Union, Washington, DC, abstract #V21A-0385.

Woods, A. W. & Koyaguchi, T. 1994. Transitions between explosive and effusive eruptions of silicic magmas. *Nature*, **370**, 641–644.

Wright, R., De La Cruz-Reyna, S., Flynn, L. P., Harris, A. J. L. & Gomez-Palacios, J. J. 2002*a*. Infrared satellite monitoring of Popocatépetl: explosions, exhalations and cycles of dome growth. *Journal of Geophysical Research*, **107**, 1–5, http://doi.org/10.1029/2000JB000125

Wright, R., Flynn, L., Garbeil, H., Harris, A. & Pilger, E. 2002*b*. Automated volcanic eruption detection using MODIS. *Remote Sensing of the Environment*, **82**, 135–155.

Wright, R., Flynn, L. P., Garbeil, H., Harris, A. J. L. & Pilger, E. 2004. MODVOLC: near-real-time thermal monitoring of global volcanism. *Journal of Volcanology and Geothermal Research*, **135**, 29–49.

Wright, R., Carn, S. A. & Flynn, L. P. 2005. A satellite chronology of the May–June 2003 eruption of Anatahan volcano. *Journal of Volcanology and Geothermal Research*, **146**, 102–116.

Yamaguchi, Y., Kahle, A., Tsu, H., Kawakami, T. & Pniel, M. 1998. Overview of advanced spaceborne thermal emission and reflectance radiometer (ASTER). *IEEE Transactions on Geoscience and Remote Sensing*, **36**, 1062–1071.